



3D structure of anisotropic flow in small collision systems at energies available at the BNL Relativistic Heavy Ion Collider

Wenbin Zhao ¹, Sangwook Ryu,¹ Chun Shen ^{1,2} and Björn Schenke³

¹*Department of Physics and Astronomy, Wayne State University, Detroit, Michigan 48201, USA*

²*RIKEN BNL Research Center, Brookhaven National Laboratory, Upton, New York 11973, USA*

³*Physics Department, Brookhaven National Laboratory, Upton, New York 11973, USA*



(Received 9 December 2022; accepted 22 December 2022; published 6 January 2023)

We present (3+1)-dimensional [(3+1)D] dynamical simulations of asymmetric nuclear collisions at the BNL Relativistic Heavy Ion Collider (RHIC). Employing a dynamical initial state model coupled to (3+1)D viscous relativistic hydrodynamics, we explore the rapidity dependence of anisotropic flow in the RHIC small system scan at 200 GeV center-of-mass energy. We calibrate parameters to describe central $^3\text{He} + \text{Au}$ collisions and make extrapolations to $d + \text{Au}$ and $p + \text{Au}$ collisions. Our calculations demonstrate that approximately 50% of the $v_3(p_T)$ difference between the measurements by the STAR and PHENIX Collaborations can be explained by the use of reference flow vectors from different rapidity regions. This emphasizes the importance of longitudinal flow decorrelation for anisotropic flow measurements in asymmetric nuclear collisions, and the need for (3+1)D simulations. We also present results for the beam energy dependence of particle spectra and anisotropic flow in $d + \text{Au}$ collisions.

DOI: [10.1103/PhysRevC.107.014904](https://doi.org/10.1103/PhysRevC.107.014904)

I. INTRODUCTION

Ultrarelativistic collisions of heavy ions are expected to create nucleus-sized droplets of quark-gluon plasma (QGP), providing a unique opportunity to study the properties of nuclear matter at extreme densities and temperatures. Precise measurements of various flow observables performed at the BNL Relativistic Heavy Ion Collider (RHIC) and the CERN Large Hadron Collider (LHC) together with the successful descriptions by hydrodynamic calculations have revealed that the created QGP fireball behaves like a nearly perfect fluid with very small specific shear viscosity [1–4]. Over the past ten years, experiments and theorists have employed multiple techniques to assess whether such QGP droplets are also formed in smaller collisions, such as $p + A$, $p + p$, and even $\gamma^* + A$ collisions [5–7] (see [8–13] for reviews), and indeed, striking features of collective expansion have been observed in high-multiplicity events of the small collision systems studied at RHIC [14,15] and the LHC [8,11,16].

At RHIC, collisions of proton (p), deuteron (d), and helium-3 (^3He) projectiles on gold (Au) targets were proposed to discern whether “flowlike” patterns are indeed geometry driven and possibly attributable to mini QGP droplet formation. The PHENIX Collaboration [15] has reported a large set of elliptic (v_2) and triangular (v_3) azimuthal anisotropy coefficients for $p + \text{Au}$, $d + \text{Au}$, and $^3\text{He} + \text{Au}$ systems. PHENIX data clearly show the hierarchy of v_2 and v_3 expected based on the differences in initial geometry between the three systems.

These collective features can be quantitatively reproduced by (2+1)-dimensional [(2+1)D] viscous hydrodynamic calculations [17,18], which translate the initial spatial anisotropies into final momentum anisotropies of produced

hadrons via the collective expansion of the bulk matter. In contrast, calculations based solely on initial-state correlations in the color glass condensate framework [19,20] are ruled out by the PHENIX data as they predict the opposite hierarchy of v_2 between the systems. Recently, the STAR Collaboration also reported measurements of the differential elliptic flow and triangular flow coefficients in these three small systems [21,22]. STAR preliminary results show that the observed $v_3(p_T)$ are system independent, different from the PHENIX published data. In [21,22] subnucleon fluctuations are emphasized to play an important role in the initial geometry and modify the expectation for the hierarchy between the flow coefficients in the different systems.

An important difference between the PHENIX and STAR analyses is the use of different pseudorapidity ranges in the two-particle correlation measurements that yield the azimuthal anisotropy coefficients. PHENIX measures the two-particle correlations between the backward rapidity ($-3.9 < \eta < -3.1$) and midrapidity regions ($-0.35 < \eta < 0.35$) with the event plane method [15,23]. In contrast, STAR employs only the mid-rapidity ($-0.9 < \eta < 0.9$) region, using the scalar-product method [21,22]. It is already well known that, in small asymmetric systems, longitudinal decorrelations are significant [24] and boost invariance is strongly broken [6,25–29]. More recent calculations also indicate that preequilibrium evolution, in either the weak [12] or strong coupling [30] limit, has a significant effect on the small and short-lived systems.

In this work, we include the effects of pre-equilibrium evolution and perform full (3+1)D hydrodynamic simulations, which we argue are essential when seeking meaningful quantitative comparisons to experimental data.

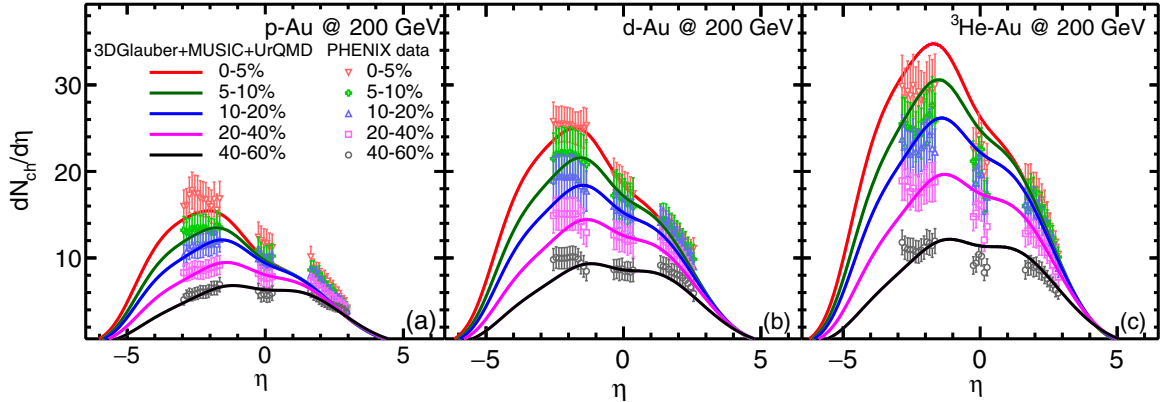


FIG. 1. The charged hadron pseudorapidity distributions $dN_{ch}/d\eta$ in various multiplicity classes of $p+Au$, $d+Au$, and ${}^3He+Au$ collisions at $\sqrt{s_N} = 200$ GeV from the 3D-GLAUBER+MUSIC+URQMD simulations, compared to experimental data from the PHENIX Collaboration [23].

More specifically, we employ a (3+1)D framework combining a dynamic initial state with hydrodynamics and hadronic transport [31] to explore the collective features in small asymmetric systems. The framework has been shown to provide a unified and quantitative description of identified hadron production in γ^* -nucleus, proton-proton, proton-nucleus, and nucleus-nucleus collisions at center-of-mass energies from a few GeV to several TeV [6,31]. Here we present detailed results on $dN_{ch}/d\eta$, mean transverse momentum ($\langle p_T \rangle$), and anisotropic flow in $p+Au$, $d+Au$, and ${}^3He+Au$ collisions in this (3+1)D hybrid hydrodynamic framework.

This paper is organized as follows: Section II briefly introduces the 3D-GLAUBER+MUSIC+URQMD model for the description of the $p/d/{}^3He+Au$ systems. Section III presents and discusses results from the 3D-GLAUBER+MUSIC+URQMD model on the $dN_{ch}/d\eta$, $\langle p_T \rangle$, and collective flow. Section IV concludes this paper with a summary.

II. THE THEORETICAL FRAMEWORK

In this paper, we employ the 3D-GLAUBER+MUSIC+URQMD hybrid model within the open-source IEBE-MUSIC framework [32] to study particle spectra and collective flow observables in $p+Au$, $d+Au$, and ${}^3He+Au$ collisions at $\sqrt{s_{NN}} = 200$ GeV, and for a range of lower beam energies in $d+Au$ collisions. The hybrid model uses a 3D Monte Carlo (MC) Glauber initial condition to dynamically deposit energy, momentum, and net baryon densities into the evolving fluid system as the two colliding nuclei are crossing each other [31,33]. The collective expansion of the QGP fireball and the evolution of the conserved net-baryon current are described by a (3+1)D viscous hydrodynamic model, MUSIC [34–38]. As the QGP expands and becomes more dilute in the hadronic phase, the fluid dynamic description is switched to a microscopic hadron cascade model, URQMD [39–41], to simulate the subsequent evolution and dynamic decoupling of the hadronic matter. More specifically, the dynamical initial condition is simulated by the 3D Monte-Carlo Glauber model on an event-by-event basis [31,33], and the space-time and momentum distributions of the initial energy-momentum tensor and net baryon charge current are provided by the classical string de-

celeration model [33,42]. The transverse positions of valence quarks and soft partonic cloud in the 3D-GLAUBER model are sampled from a 2D Gaussian, $\exp[-x^2+y^2/B_G^2]$, with a transverse nucleon width parameter $B_G = 5 \text{ GeV}^{-2}$, corresponding to a nucleon width of $w = 0.44$ fm. After the collision, the deposited energy density distribution has a Gaussian profile in the transverse plane with a width of $w_q = 0.2$ fm. We parametrize the average rapidity loss function of the valence quarks and the soft partonic cloud with their incoming rapidity y_{init} in the collision pair rest frame as [31,43]

$$\langle y_{loss} \rangle(y_{init}) = A y_{init}^{\alpha_2} [\tanh(y_{init})]^{\alpha_1 - \alpha_2}. \quad (1)$$

As shown in Fig. 1, when choosing the three parameters values $A = 1.32$, $\alpha_1 = 1.8$, and $\alpha_2 = 0.34$, we can reproduce the measured pseudo-rapidity distributions of charged hadrons for $p+Au$, $d+Au$, and ${}^3He+Au$ collisions at $\sqrt{s_{NN}} = 200$ GeV. The spatial topography of the deuteron's two-nucleon system is obtained from sampling the Hulthen wave function [44], and fluctuating 3He configurations come from results of Green's function Monte Carlo calculations using the AV18+UIX model interaction [45]. The detailed implementation of this initial condition model is discussed in Ref. [31].

To incorporate the effects of prehydrodynamic flow, we include a finite transverse initial velocity motivated by the blast-wave model [46–48]. We assume the initial flow is radial and its strength is characterized by the transverse flow rapidity,

$$\eta_{\perp} = \alpha^{\text{pre-flow}} r, \quad (2)$$

where r is the radial distance from the string center. The $\alpha^{\text{pre-flow}}$ parameter controls the strength of the prehydrodynamic flow. Here we set $\alpha^{\text{pre-flow}} = 0.15$ to fit the $v_n(p_T)$ in ${}^3He+Au$ at 200 GeV. We will explore the effects of prehydrodynamic flow on hadronic observables in $p+Au$ collisions in Appendix B.

The produced strings from individual nucleon-nucleon collisions are treated as dynamical source terms for the hydrodynamic evolution [31,33,49–51],

$$\partial_{\mu} T^{\mu\nu} = J^{\nu}, \quad (3)$$

$$\partial_{\mu} J_B^{\mu} = \rho_B. \quad (4)$$

Here we use a crossover equation of state (NEOS-BQS) for the QCD matter at finite chemical potentials, that is constructed using recent lattice data [52–56]. We employ the strangeness neutrality condition, $n_s = 0$, and for simplicity set the net electric charge-to-baryon density ratio to $n_Q/n_B = 0.4$ [56], a value most appropriate for large nuclei. The specific shear and bulk viscosities are parametrized as

$$\frac{\eta T}{e + P} = (\eta/s)_{\text{norm}} \left[1 + (\eta/s)_{\text{slope}} \left(\frac{\mu_B}{\mu_{B,\text{scale}}} \right)^\alpha \right], \quad (5)$$

$$\frac{\zeta T}{e + P} = (\zeta/s)_{\text{norm}} \exp \left[- \left(\frac{T - T_{\text{peak}}}{T_{\text{width}, \leq}} \right)^2 \right], \quad (6)$$

where $T_{\text{width}, <} = 0.015$ GeV for $T < T_{\text{peak}}$, and $T_{\text{width}, >} = 0.1$ GeV for $T > T_{\text{peak}}$ with $T_{\text{peak}} = 0.17$ GeV and $(\zeta/s)_{\text{norm}} = 0.08$. For the specific shear viscosity, we set $(\eta/s)_{\text{norm}} = 0.13$, $(\eta/s)_{\text{slope}} = 1.0$, $\mu_{B,\text{scale}} = 0.6$ GeV, and $\alpha = 1.5$. The shear stress tensor and bulk viscous pressure are evolved with the Denicol-Niemi-Molnár-Rischke (DNMR) theory with spatial gradients up to the second order [37,57]. For simplicity, the effect of charge diffusion is neglected in this work. These transport coefficients are chosen to reproduce the mean transverse momentum and the differential flow in central $^3\text{He} + \text{Au}$ collisions at 200 GeV. In addition, the μ_B dependence of η/s is informed by calibrating flow observables in Au+Au collisions from 7.7 to 200 GeV [58]. Compared to Ref. [31], we use smaller sizes for nucleons and hotspots, which are consistent with the subnucleonic structure constrained by a recent Bayesian analysis [59]. The small hotspot size ($w_q = 0.2$ fm) and inclusion of pre-hydrodynamic flow require a nonzero QGP bulk viscosity in the hydrodynamic evolution, which was neglected in [31].

In the IEBE-MUSIC framework, the Cooper-Frye particleization of the fluid cells is performed on a hypersurface with a constant energy density of $e_{\text{sw}} = 0.50$ GeV/fm³ using the Cornelius algorithm [60] and the open-source code package ISS [61,62]. The nonequilibrium shear and bulk viscosity corrections to the local equilibrium distribution function are taken from Grad's moments method with multiple conserved charges [58]. The produced hadrons are then fed into the hadron cascade model, URQMD, for further scatterings and decays until kinetic freeze-out is achieved dynamically.

III. RESULTS

In this section, we report results for observables, including charged hadron pseudorapidity distributions, mean transverse momentum, and differential flow harmonics for the $p + \text{Au}$, $d + \text{Au}$, and $^3\text{He} + \text{Au}$ collision systems at RHIC energies.

A. Charged hadron multiplicity rapidity distribution and average transverse momentum

Figure 1 shows the charged hadron pseudorapidity distributions in different centrality bins for $p + \text{Au}$, $d + \text{Au}$, and $^3\text{He} + \text{Au}$ collisions at $\sqrt{s_{NN}} = 200$ GeV. We note that all parameters were tuned to reproduce observables in $^3\text{He} + \text{Au}$ collisions. Keeping all the model parameters fixed, our

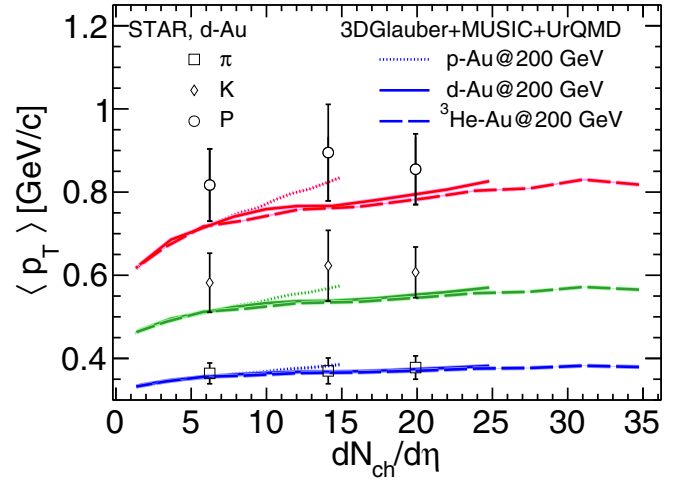


FIG. 2. Identified particle mean transverse momenta $\langle p_T \rangle$ as functions of charged hadron multiplicity in $p + \text{Au}$ (solid lines), $d + \text{Au}$ (dotted lines), and $^3\text{He} + \text{Au}$ (dashed lines) collisions from the 3D-GLAUBER+MUSIC+URQMD framework. The $d + \text{Au}$ results are compared to experimental data from the STAR Collaboration [65].

model's extrapolations provide a reasonable description of the experimental data from the PHENIX Collaboration [23] for the $p + \text{Au}$ and $d + \text{Au}$ systems. In particular, the increase of the asymmetry around midrapidity from peripheral to central collisions is well captured as a consequence of the increasing number of participant nucleons from the Au target towards central collisions. Here we have used the charged hadron multiplicity in the pseudorapidity range $-3.9 < \eta < -3.1$ (in the Au-going direction) to determine the collision centrality bins, which is consistent with the method used by PHENIX [23]. As pointed out in Ref. [31], the correlation of particle production between forward and midrapidity is crucial to reproduce the centrality dependence of charged particles in these asymmetric collision systems. This is highlighted in Fig. 10 in Appendix A, where we show that using different centrality definitions generates different shapes for $dN_{ch}/d\eta$.

Within the hydrodynamic paradigm, the mean transverse momentum of identified hadrons strongly constrains the radial expansion of the fireball. This radial expansion is very sensitive to the bulk viscosity, initial hotspot size, and the strength of prehydrodynamic flow. Consequently, the mean transverse momentum provides a strong constraint on $(\zeta/s)(T)$ [63,64]. In Fig. 2 we show the identified particle mean transverse momentum as a function of charged hadron multiplicity in $p + \text{Au}$, $d + \text{Au}$, and $^3\text{He} + \text{Au}$ collisions at 200 GeV and compare to the STAR measurements for $d + \text{Au}$ collisions [65]. Using the temperature-dependent bulk viscosity $(\zeta/s)(T)$ in Eq. (6) with $(\zeta/s)_{\text{norm}} = 0.08$, the calculation shows good agreement with the STAR data in $d + \text{Au}$ collisions [65]. This indicates that our hybrid model simulations generate proper amounts of radial flow and the transverse expansion has been well constrained.

The flow harmonics describe the momentum anisotropy of the final produced hadrons. They are commonly measured using the two-particle correlation method with a large pseudorapidity gap between the particles to suppress nonflow

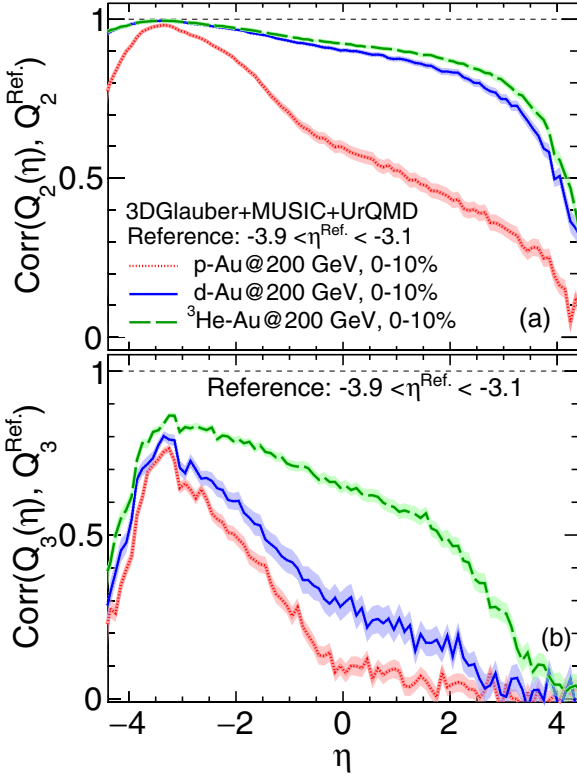


FIG. 3. The correlation between the flow vectors as a function of pseudo-rapidity η with the reference vector calculated within $-3.9 < \eta^{\text{Ref.}} < -3.1$ in p +Au, d +Au, and ${}^3\text{He}$ +Au systems from the 3D-GLAUBER+MUSIC+URQMD simulations.

correlations [66,67]. The presence and size of the gap will affect the measured value of $v_n\{2\}$ if the correlation between the flow vectors depends on the pseudorapidity separation of two particles. Therefore, we calculate the η -dependent correlations between the flow vectors Q_n defined by

$$\text{Corr}(Q_n(\eta), Q_n^{\text{Ref.}}) = \frac{\langle Q_n^*(\eta) Q_n^{\text{Ref.}} \rangle}{\sqrt{\langle |Q_n(\eta)|^2 \rangle} \sqrt{\langle |Q_n^{\text{Ref.}}|^2 \rangle}}, \quad (7)$$

to characterize the longitudinal decorrelation of flow vectors. Here, $Q_n(\eta)$ is the n th order flow vector defined in the η bin of interest, and $Q_n^{\text{Ref.}}$ is the n th order reference flow vector within the assigned reference η range. Figure 3 shows the correlation $\text{Corr}(Q_n(\eta), Q_n^{\text{Ref.}})$ of the second- and third-order flow vectors with their reference flow vectors calculated within $-3.9 < \eta < -3.1$ in central 0–10% p +Au, d +Au, and ${}^3\text{He}$ +Au systems, following PHENIX’s detector coverage [15].

The values of $\text{Corr}(Q_n(\eta), Q_n^{\text{Ref.}})$ for $|\eta| < 0.35$ show the strength of flow vector correlations relevant for the PHENIX measurement of $v_n\{2\}$ [15]. For elliptic flow, we find that the correlation drops slowly with pseudorapidity and is approximately 0.9 for $|\eta| < 0.35$ in d +Au and ${}^3\text{He}$ +Au collisions. However, the flow vector correlation drops quite rapidly in p +Au collisions, reaching ≈ 0.6 in the $|\eta| < 0.35$ bin, which indicates that the $v_2\{2\}$ measurements could depend strongly on the rapidity regions used in the analysis. For the triangu-

lar flow coefficients, the flow correlations are significantly below unity for all three systems and drop more rapidly with η compared to the case of $n = 2$. This result demonstrates that it is nontrivial to extract the fireball’s initial triangularity hierarchy from $v_3\{2\}$ measurements. Because the boost-invariant (2+1)D simulations cannot capture these longitudinal flow correlations, their results for triangular flow in $(p, d, {}^3\text{He})$ +Au collisions are highly idealized and contain substantial theoretical uncertainties.

The three panels of Fig. 4 show the elliptic flow $v_2(\eta)$ as a function of pseudorapidity in the 0–5% centrality bin of $\sqrt{s_{NN}} = 200$ GeV p +Au, d +Au, and ${}^3\text{He}$ +Au collisions, respectively. Following the same method as used by the PHENIX Collaboration [23], we calculate the second flow harmonic, $v_2(\eta)$, using the event plane (EP) method with the event plane determined in the range $-3.9 < \eta < -3.1$, corresponding to using the Beam Beam Counter (BBC) in the Au-going direction, and with centrality defined by the charged hadron multiplicity measured in the same range. The flow harmonics for the event plane method are calculated using

$$v_n(\eta, p_T)\{\text{EP}\} = \frac{\langle \cos [n(\phi(\eta, p_T) - \Psi_n^{\text{Ref.}})] \rangle}{R(\Psi_n^{\text{Ref.}})}, \quad (8)$$

where $\phi(\eta, p_T)$ is the azimuthal angle of particles of interest for specific η and/or p_T bins, $\Psi_n^{\text{Ref.}}$ is the n th order azimuthal reference event plane, and $R(\Psi_n^{\text{Ref.}})$ is the resolution of $\Psi_n^{\text{Ref.}}$. Following the PHENIX measurements [14,23,68], the event plane resolution is estimated by

$$R(\Psi_n^{\text{Ref.}}) = \sqrt{\frac{\langle \frac{Q_{nA}}{|Q_{nA}|} \frac{Q_{nB}^*}{|Q_{nB}|} \rangle \langle \frac{Q_{nA}}{|Q_{nA}|} \frac{Q_{nC}^*}{|Q_{nC}|} \rangle}{\langle \frac{Q_{nB}}{|Q_{nB}|} \frac{Q_{nC}^*}{|Q_{nC}|} \rangle}}, \quad (9)$$

with the n th-order flow vector

$$Q_n = \sum_k e^{in\phi_k}, \quad (10)$$

with the \sum summing over particles in one event. The $Q_{nA,B,C}$ vectors are defined in the $-3.9 < \eta < -3.1$ (south BBC, Au-going side), $-3.0 < \eta < -1.0$ [south Forward Silicon Vertex (FVTX)], and $|\eta| < 0.35$ (central, CNT), respectively. The 3D-GLAUBER+MUSIC+URQMD model gives a reasonable description of the η -dependent elliptic flow in d +Au and ${}^3\text{He}$ +Au systems. Both the experimental data and our model simulations have an increasing flow coefficient v_2 towards backward rapidity up to $\eta = -3.0$ in the Au-going direction. At $\eta < -3.0$, our model predicts a decrease of $v_2(\eta)$. The $v_2(\eta)$ of ${}^3\text{He}$ +Au is slightly larger than that of d +Au collisions because of the longer fireball lifetime in the hydrodynamic phase in ${}^3\text{He}$ +Au collisions. For the p +Au system, the PHENIX data show a pronounced increase of the $v_2(\eta)$ towards negative rapidities, especially for $\eta < -2.0$. Our model fails to describe the $v_2(\eta)$ for $\eta < 1.0$ in p +Au collisions. We expect $v_2(\eta)$ in p +Au collisions to be smaller than in the other systems because of the stronger decorrelation and in p +Au collisions, compared to d +Au and ${}^3\text{He}$ +Au collisions, as shown in Fig. 3. Also the shorter lifetime in p +Au collisions can lead to smaller $v_2(\eta)$.

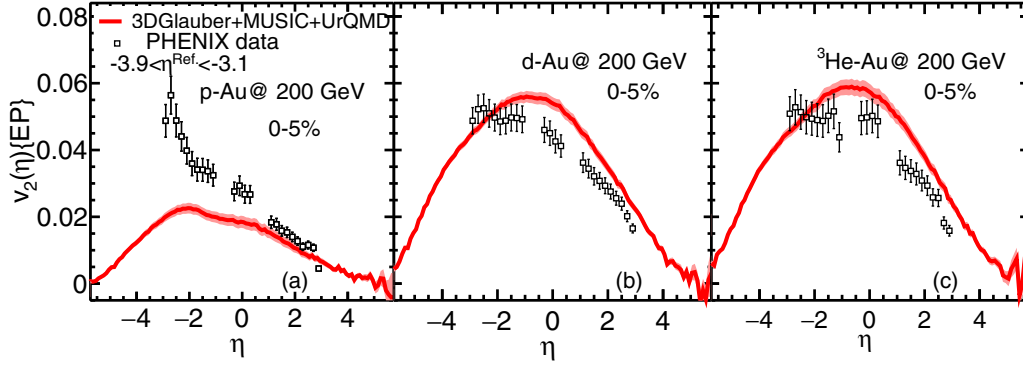


FIG. 4. Elliptic flow v_2 as a function of pseudorapidity (η) in high-multiplicity 0–5% central p +Au, d +Au, and ^3He +Au collisions at $\sqrt{s_{NN}} = 200$ GeV from the 3D-GLAUBER+MUSIC+URQMD framework. The results are compared to the experimental data from the PHENIX Collaboration [23].

Figure 5 shows the computed p_T -differential flow $v_n(p_T)$ ($n = 2, 3$) for charged hadrons compared to experimental data from the PHENIX and STAR Collaborations. Here, we adopt the same methods and kinematic cuts as employed in the PHENIX or STAR analyses, respectively. Specifically, when comparing to the PHENIX data [15], we select collision events for 0–5% centrality using the number of charged hadrons in $\eta \in [-3.9, -3.1]$. The $v_n(p_T)$ [EP] (PHENIX) for charged hadrons in the midrapidity region covering $|\eta| < 0.35$ (central, CNT) are calculated with the event plane method by Eq. (8), where the second-order event plane is determined in the Au-going direction, in the pseudorapidity range $-3.0 < \eta < -1.0$ (south FVTX) in p/d +Au and $-3.9 < \eta < -3.1$ (south BBC) in ^3He +Au collisions, and the third-order event planes are determined in the range of the south BBC for all systems [15]. The event plane resolutions are calculated with the three-subevent method, which correlates measurements in the south BBC, south FVTX, and central CNT arms [15,23] as given explic-

itly in Eq. (9). The centrality classes are defined using the multiplicity of charged hadrons in the pseudorapidity range $-3.9 < \eta < -3.1$.

To compare with the experimental data from the STAR Collaboration [21,22], we select the 0–2% most central p +Au collisions and 0–10% most central d +Au and ^3He +Au collisions, based on the charged hadron multiplicity in $\eta \in [-0.9, 0.9]$. The STAR flow measurements imposed a rapidity gap $|\Delta\eta| > 1$ for charged particles in $\eta \in [-0.9, 0.9]$. For convenience we compute the two-particle flow coefficients using the scalar-product (SP) method with particles of interest (POIs) and reference particles (RPs) selected from two subevents within $-0.9 < \eta < -0.5$ and $0.5 < \eta < 0.9$, respectively. We confirmed that this approximates STAR’s method very well.

As mentioned above, we tune parameters to fit observables, including $v_2(p_T)$ and $v_3(p_T)$, in ^3He +Au collisions, and then predict observables in p +Au and d +Au collisions. Figure 5 shows that the 3D-GLAUBER+MUSIC+URQMD model gives an

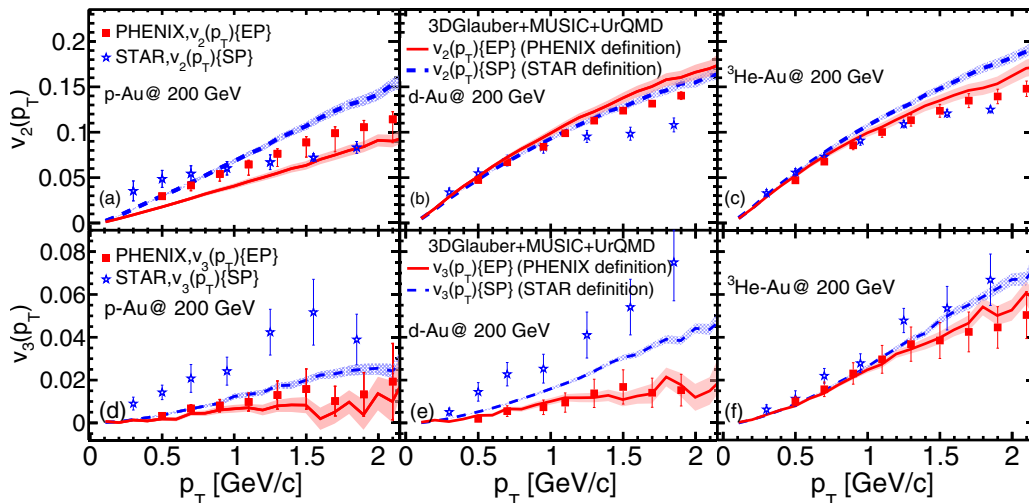


FIG. 5. The anisotropic flow $v_n(p_T)$ as a function of p_T in central p +Au, d +Au, and ^3He +Au collisions computed from the 3D-GLAUBER+MUSIC+URQMD framework. The results are compared to the experimental data from the PHENIX and STAR Collaborations [15,21]. The PHENIX data are all 0–5% and STAR data are 0–2%, 0–10%, and 0–10% for p +Au, d +Au, and ^3He +Au collisions, respectively.

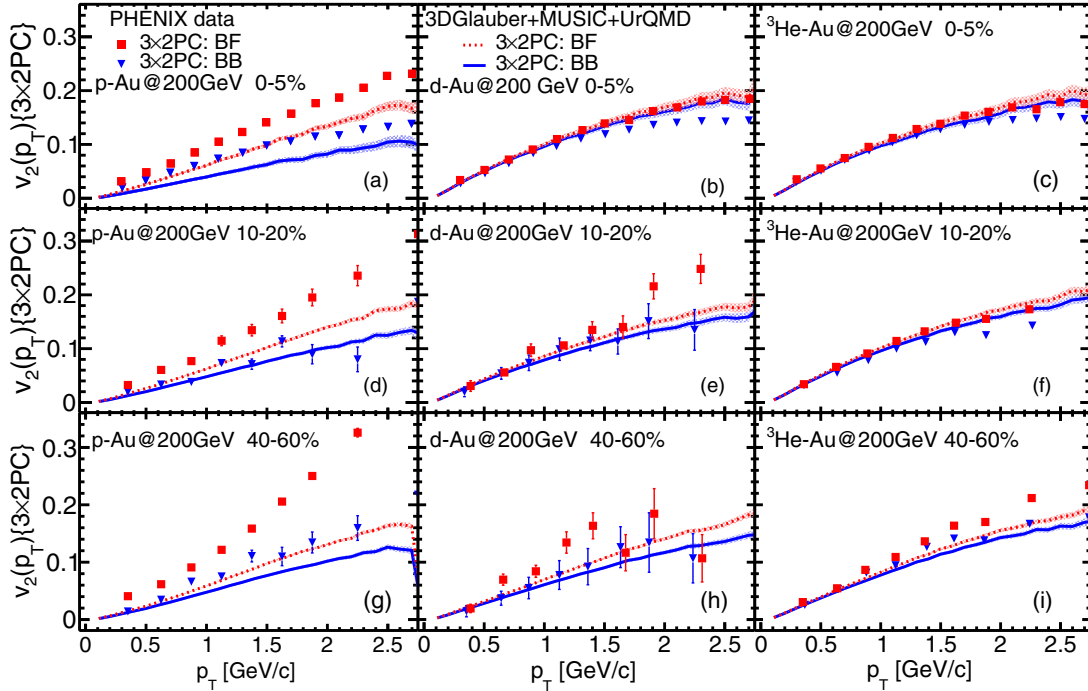


FIG. 6. The differential elliptic flow $v_2(p_T)$ in ${}^3\text{He}/d/p+\text{Au}$ collisions at $\sqrt{s_{NN}} = 200$ GeV determined by the $3 \times 2\text{PC}$ method using pseudorapidity ranges corresponding to the FVTXS-CNT-FVTXN (BF) and BBCS-FVTXS-CNT (BB) detector combinations. The model results are compared to experimental data from the PHENIX Collaboration [69,70]

overall good description of the PHENIX $v_n(p_T)$ data for $d+\text{Au}$ and ${}^3\text{He}+\text{Au}$ collisions. We underestimate the $v_2(p_T)$ in $p+\text{Au}$ collisions by about 20–30%, possibly because of a too large longitudinal flow decorrelation in the model. Compared to the STAR elliptic flow, our model provides a reasonable description for $p_T < 1$ GeV for $(d, {}^3\text{He})+\text{Au}$ collisions, but underestimates the data for $p+\text{Au}$ collisions. Our calculation overestimates the STAR $v_2(p_T)$ at higher p_T . The STAR $v_3(p_T)$ measurements show a much weaker system size dependence than the model, which gives a good description of $v_3(p_T)$ in ${}^3\text{He}+\text{Au}$ but significantly underestimates $v_3(p_T)$ in $(p, d)+\text{Au}$ collisions.

Both in the model calculations and experimental data, the $v_3(p_T)$ with the STAR definition (stars) are systemically larger than those determined using the PHENIX definition (squares). In our calculations, this difference is mainly caused by the different magnitudes of the longitudinal decorrelation of flow vectors of v_3 between the different pseudorapidity bins. That is, the decorrelation between the flow vectors at $-3.9 < \eta < -3.1$ and $-0.35 < \eta < 0.35$ is greater than that between $-0.9 < \eta < -0.5$ and $0.5 < \eta < 0.9$.

However, our model still underestimates the STAR data of $v_3(p_T)$ in $p+\text{Au}$ and $d+\text{Au}$ collisions, indicating that the decorrelations present in the model do not fully account for the differences between the STAR and PHENIX results. We leave a more systematic calibration of fitting both STAR and PHENIX data for future studies using a Bayesian framework. This study should shed more light on the role of any residual nonflow in the experimental data.

Recently, the PHENIX Collaboration measured anisotropic flow coefficients using the $3 \times 2\text{PC}$ method, whose two-

particle azimuthal correlations are constructed with three different sets of pairs [69,70]. Taking the p_T -integrated flow vector $Q_{nA,B,C}$, and the p_T -differential flow vector $q_{nA,B,C}(p_T)$ of particles of interest (using finite p_T bins) from different subevents A, B , and C that indicate different pseudorapidity bins, the differential $v_n(p_T)$ of the particles of interest in the single subevent C can be determined as

$$v_n^C(p_T) = \sqrt{\frac{c_n^{AC}(p_T)c_n^{BC}(p_T)}{C_n^{AB}}}, \quad (11)$$

where the p_T -differential $c_n(p_T)$ and p_T -integrated C_n coefficients are defined as

$$C_n^{AB} = \langle Q_{nA}Q_{nB}^* \rangle, \quad (12)$$

$$c_n^{AC}(p_T) = \langle Q_{nA}q_{nC}^*(p_T) \rangle, \quad (13)$$

$$c_n^{BC}(p_T) = \langle Q_{nB}q_{nC}^*(p_T) \rangle. \quad (14)$$

Here $\langle \dots \rangle$ represents event averaging and taking the real part of the correlator.

Figure 6 shows the differential elliptic flow $v_2(p_T)\{3 \times 2\text{PC}\}$ at midrapidity $|\eta| < 0.35$ in ${}^3\text{He}+\text{Au}$, $d+\text{Au}$, and $p+\text{Au}$ systems, respectively. Following the PHENIX measurements [69,70], we calculate the $v_2(p_T)$ from the $3 \times 2\text{PC}$ method with two combinations: “ $-3.0 < \eta < -1.0$, $-0.35 < \eta < 0.35$, and $1.0 < \eta < 3.0$,” FVTXS-CNT-FVTXN, detector combination (BF); and “ $-3.9 < \eta < -3.1$, $-3.0 < \eta < -1.0$, and $-0.35 < \eta < 0.35$,” BBCS-FVTXS-CNT, detector combination (BB).

The 3D-GLAUBER+MUSIC+URQMD model reproduces the $v_2(p_T)\{3 \times 2\text{PC}\}$ in $d+\text{Au}$ and ${}^3\text{He}+\text{Au}$ collisions quite well

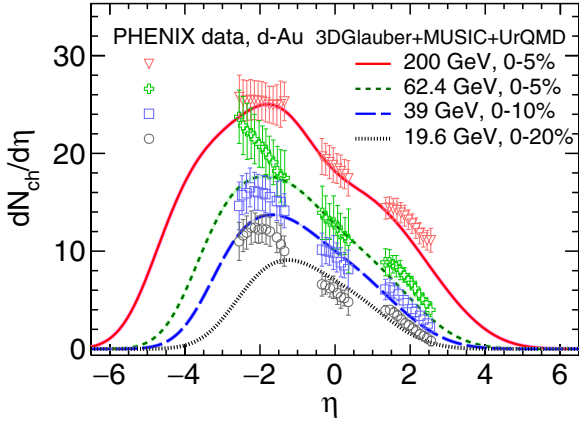


FIG. 7. The charged hadron pseudorapidity distributions $dN_{ch}/d\eta$ of central $d+Au$ collisions at $\sqrt{s_{NN}} = 200, 62.4, 39,$ and 19.6 GeV from the 3D-GLAUBER+MUSIC+URQMD simulations, compared to experimental data from the PHENIX Collaboration [68].

up to 60% in centrality. The model calculations produce a slowly decreasing trend in $v_2(p_T)$'s magnitude from central to peripheral collisions for both the BF and BB combinations. This trend is caused by the shorter hydrodynamic lifetimes in more peripheral collisions. More importantly, our model quantitatively reproduces the difference between $v_2(p_T)$ (BF) and $v_2(p_T)$ (BB), which suggests that our model predicts the right amount of longitudinal flow decorrelation in $d+Au$ and ^3He+Au collisions from most central to middle central collisions. Our model results underestimate the measurements in the peripheral collisions, for example in 40-60% bin, where we expect sizable nonflow correlations in the measurements.

Similar to the previous $v_n\{2\}$ comparison, our calculations underestimate the $p+Au$ $v_2(p_T)$ by 40% across all centrality bins. Interestingly, our model can reasonably reproduce the difference between $v_2(p_T)$ (BF) and $v_2(p_T)$ (BB) in 0-5% and 10-20% central $p+Au$ collisions. Furthermore, this $v_2(p_T)$ difference between BF and BB is larger in $p+Au$ collisions than in $(d, ^3He)+Au$ collisions, suggesting a large longitudinal flow decorrelation in $p+Au$ collisions, as is present in our model. The PHENIX $v_2(p_T)$ (BF) for 40%-60% $p+Au$ collisions show rapid increases at high p_T , suggesting sizable residual nonflow correlations.

B. Results for the $d+Au$ Beam Energy Scan

In this subsection, we extrapolate our model to $d+Au$ collisions at lower collision energies. To do so we only reduce the center-of-mass collision energy and keep all model parameters fixed.

Figure 7 shows our model predictions for the collision energy dependence of the charged hadron pseudorapidity distribution in central $d+Au$ collisions. Our model gives an overall good description of the asymmetric charged hadron pseudorapidity distributions compared with the PHENIX data from $\sqrt{s_{NN}} = 200$ to 19.6 GeV. The peaks of $dN_{ch}/d\eta$ in the theoretical calculations are shifted more towards midrapidity compared with the PHENIX measurements at low collision

energies, suggesting a small overestimation of the rapidity loss in the initial-state model for the lower collision energies. Compared to the results shown in Ref. [31], the current $dN_{ch}/d\eta$ at 19.6 GeV is slightly smaller because a higher switching energy density $e_{sw} = 0.5$ GeV/fm³ is used here for all collision energies.

Figure 8 shows the model-to-data comparisons for $v_2\{2\}$, $v_2\{4\}$, and $v_2\{2, |\Delta\eta| > 2.0\}$ in $d+Au$ collisions at 200, 62.4, 39, and 19.6 GeV, using the PHENIX FVTX ($1.0 < |\eta| < 3.0$) acceptance [14]. Here, following the PHENIX measurements [14,71], the N_{Track} is estimated by $N_{Track} = p_0 \times N_{ch}$, with $p_0 = 0.67$ being the tracking efficiency and acceptance in the FVTX detector. The N_{ch} is the charged hadron multiplicity within the FVTX acceptance $1 < |\eta| < 3$ computed in our model. With a rapidity gap of $|\Delta\eta| > 2.0$, nonflow correlations can be effectively suppressed.

We find our calculations agree nicely with the PHENIX $v_2\{2, |\Delta\eta| > 2.0\}$ data for all four collision energies. The difference between $v_2\{2\}$ and $v_2\{2, |\Delta\eta| > 2.0\}$ data indicate the contributions from event plane decorrelation and nonflow correlations. In our calculations, the difference between these two correlation observables only comes from the event plane decorrelations. Therefore, the difference between the model and PHENIX $v_2\{2\}$ can serve as an estimation of nonflow correlations in the measurements.

The elliptic flow measured using the four-particle cumulant method, $v_2\{4\}$, in general, contains fewer non-flow correlations. Our model results overestimate $v_2\{4\}$ for central $d+Au$ collisions at 200 GeV. For the lower collision energies, our $v_2\{4\}$ underestimates the PHENIX data. At the current stage, it is not clear whether the discrepancy originates from possible residual nonflow correlation in the measurements or different variances in the elliptic flow distributions.

Finally, Fig. 9 shows the rapidity-dependent $v_2(\eta)\{EP\}$ in central $d+Au$ collisions at $\sqrt{s_{NN}} = 200, 62.4, 39,$ and 19.6 GeV, calculated using the same event plane method as that in Fig. 4. Our model produces results close to the PHENIX measurements at the top three collision energies. Our $v_2(\eta)\{EP\}$ at 19.6 GeV serves as a model prediction. The $v_2(\eta)\{EP\}$ at all four energies have similar shapes with respect to $dN_{ch}/d\eta$ that decreases with increasing η between $0 < \eta < 3$ in the proton-going side, and peaks at the Au-going side. This correlation between $v_2(\eta)$ and $dN_{ch}/d\eta$ reflects that the size of the elliptic flow is proportional to the fireball lifetime in the hydrodynamic phase [68].

IV. SUMMARY

We explored the collectivity in asymmetric ($p, d, ^3He$)+Au collisions at 200 GeV and $d+Au$ collisions at 19.6-200 GeV within a (3+1)D hybrid theoretical framework. We find that the elliptic flow vector correlations in the PHENIX kinematic regions remain ≈ 0.9 for central ($d, ^3He$)+Au collisions at 200 GeV, ensuring a good signal of the geometric response from initial 2D ellipticity to final-state charged hadron elliptic flow. However, the elliptic flow correlation drops to 0.6 in central $p+Au$ collisions. For triangular flow, the flow correlations are significantly below unity for all three collision systems. The presence of

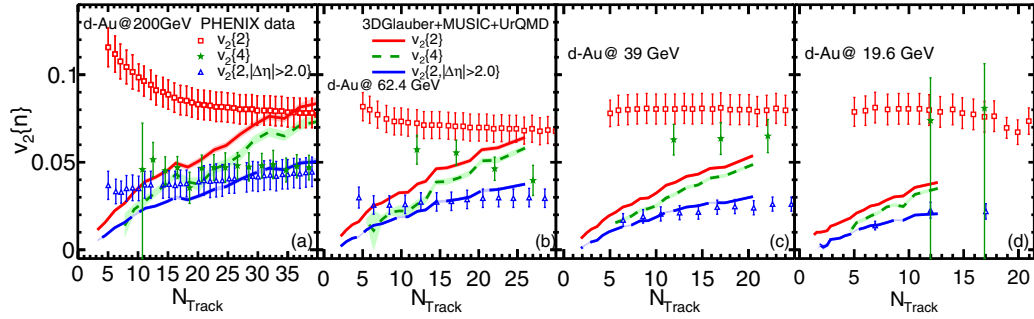


FIG. 8. Charged hadron elliptic flow $v_2\{2\}$, $v_2\{4\}$ and $v_2\{2, |\Delta\eta| > 2.0\}$ as a function of charged hadron multiplicity N_{Track} of $d+\text{Au}$ collisions at $\sqrt{s_{NN}} = 200, 62.4, 39$ and 19.6 GeV from the 3D-GLAUBER+MUSIC+URQMD framework. The results are compared to experimental data from the PHENIX Collaboration [14].

substantial flow decorrelations leads to the conclusion that full (3+1)D simulations are required for any quantitative comparisons to experimental data from these asymmetric collision systems.

With parameters calibrated using the central $^3\text{He}+\text{Au}$ measurements, the 3D-GLAUBER+MUSIC+URQMD model reproduces the PHENIX two-particle $v_n(p_T)$ in central $d+\text{Au}$ collisions, but underestimates the $p+\text{Au}$ $v_n(p_T)$ by 30%. By computing $v_n(p_T)$ using the STAR definitions, we find a 30% larger $v_3(p_T)$ with the STAR definition compared to the triangular flow from the PHENIX definition. Compared to the STAR measurements, our calculations suggest that approximately 50% of the difference between the PHENIX and STAR $v_3(p_T)$ originates from the different flow correlations between different rapidity regions. The remaining discrepancy between our calculations and the experimental data could come from different origins, including pre-hydrodynamic flow and non-flow in the experimental data that is not present in the model.

We further obtain a reasonable agreement with PHENIX measurements of differential elliptic flow using the $3 \times 2\text{PC}$ method in $d+\text{Au}$ and $^3\text{He}+\text{Au}$ collisions up to 60% in centrality. We underestimate the $v_2(p_T)$ in $p+\text{Au}$ by approximately 40%. However, our model quantitatively reproduces the difference between the $v_2(p_T)$ measured using the BF and BB combinations of detectors for all three systems. The larger observed difference between $v_2(p_T)(\text{BF})$ and $v_2(p_T)(\text{BB})$ in $p+\text{Au}$ collisions compared to ($d, ^3\text{He}$)+Au collisions

suggests a larger longitudinal flow decorrelation in $p+\text{Au}$ collisions, as present in our model.

Lastly, we extrapolate our model calculations to $d+\text{Au}$ collisions at 19.6, 39, and 62.4 GeV. With all the model parameters fixed by the $^3\text{He}+\text{Au}$ collisions at 200 GeV, our model predictions give good descriptions of PHENIX measurements of $v_2\{2\}$ with a rapidity gap and the rapidity dependent elliptic flow in $d+\text{Au}$ at the lower collision energies.

In summary, our study explicitly demonstrates that longitudinal flow decorrelations play a central role in anisotropic flow measurements in asymmetric nuclear collisions. We conclude that full (3+1)D hybrid simulations are essential for making quantitative comparisons with observables from small system collisions at RHIC.

ACKNOWLEDGMENTS

We thank Ron Belmont for providing the PHENIX data and Mashhood Munir for estimates of the pre-hydrodynamic flow. We thank Shengli Huang, Ulrich W. Heinz, Jiangyong Jia, and Zhengbu Xu for helpful discussions and suggestions. W.B.Z. is supported by the National Science Foundation (NSF) under Grants No. ACI-2004571 within the framework of the XSCAPE project of the JETSCAPE collaboration. S.R. is supported by the U.S. Department of Energy (DOE) under Grant No. DE-SC0013460. B.P.S. and C.S. are supported by the U.S.

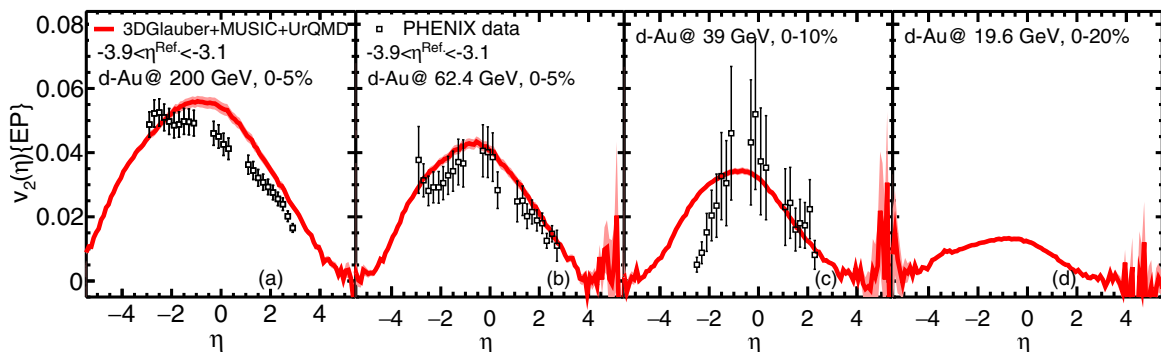


FIG. 9. Elliptic flow v_2 as a function of pseudo-rapidity in high-multiplicity central $d+\text{Au}$ collisions at $\sqrt{s_{NN}} = 200, 62.4, 39$ and 19.6 GeV from the 3D-GLAUBER+MUSIC+URQMD framework. The results are compared to the experimental data from the PHENIX Collaboration [68].

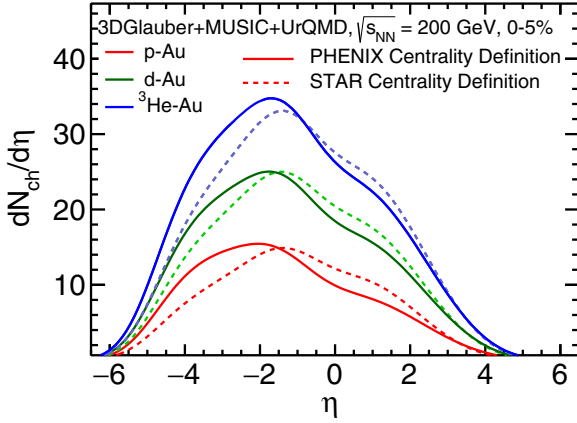


FIG. 10. The charged hadron pseudorapidity distributions $dN_{ch}/d\eta$ with different centrality selections of central p +Au, d +Au and ${}^3\text{He}$ +Au collisions at $\sqrt{s_{NN}} = 200$ GeV from the 3D-GLAUBER+MUSIC+URQMD simulations.

Department of Energy, Office of Science, Office of Nuclear Physics, under DOE Contract No. DE-SC0012704 and Award No. DE-SC0021969, respectively. C.S. acknowledges support from a DOE Office of Science Early Career Award. This work is in part supported within the framework of the Beam Energy Scan Theory (BEST) Topical Collaboration and under Contract No. DE-SC0013460. This research was done using resources provided by the Open Science Grid (OSG) [72,73], which is supported by the National Science Foundation Award No. 2030508.

APPENDIX A: CENTRALITY SELECTION DEPENDENCE OF $dN_{ch}/d\eta$ IN ASYMMETRIC COLLISIONS

We study the effects of different centrality definitions on the charged hadron pseudo-rapidity distributions in 0–5% central ($p, d, {}^3\text{He}$)+Au collisions at 200 GeV. Figure 10 shows the comparison of the $dN_{ch}/d\eta$ between the PHENIX centrality definition (determined by charged hadron multiplicity within $-3.9 < \eta < -3.1$) and the STAR centrality definition (determined by charged hadron multiplicity within $-0.9 < \eta < 0.9$). The STAR centrality definition gives a larger yield at midrapidity than that using PHENIX's definition, while the central events according to the PHENIX definition have larger yields in the backward (negative) rapidity region. Figure 10 illustrates that it is crucial to adopt the same centrality definition as the experiment for model-to-data comparisons in these asymmetric collisions, emphasizing again the need for full (3+1)d hybrid simulations.

APPENDIX B: IMPORTANCE OF PREHYDRODYNAMIC EVOLUTION FOR ANISOTROPIC FLOW IN p +Au COLLISIONS

We investigate the importance of the pre-hydrodynamic flow for hadronic observables in p +Au collisions. Figures 11 and 12 show the identified particle mean transverse momenta and the $v_n(p_T)$ ($n = 2, 3$) with different values of the α^{preflow} defined in Eq. (2) when simulating central p +Au collisions

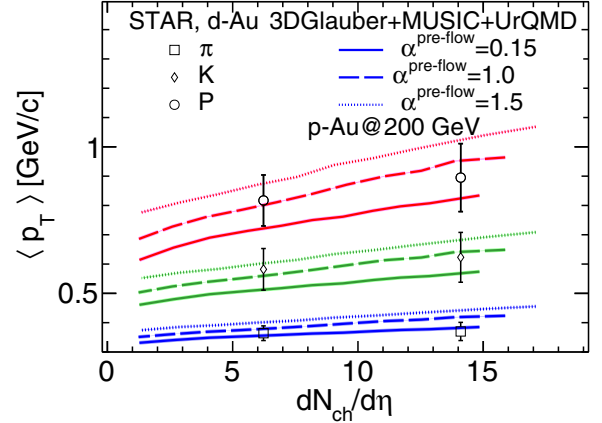


FIG. 11. Identified particle mean transverse momenta $\langle p_T \rangle$ as functions of charged hadron multiplicity in p +Au collisions with different values of α^{preflow} from the 3D-GLAUBER+MUSIC+URQMD framework. The results are compared to experimental d +Au data from the STAR Collaboration [65].

at 200 GeV. Here the α^{preflow} parameter controls the strength of the prehydrodynamic flow. Figure 11 shows that a larger pre-hydrodynamic flow leads to a faster transverse expansion, which results in larger $\langle p_T \rangle$ for identified hadrons. The proton's mean p_T shows a stronger sensitivity to α^{preflow} than that of pions and kaons. It is also noteworthy that the faster fireball expansion with a larger α^{preflow} shortens the overall fireball lifetime and its longitudinal expansion. Therefore, there is slightly more energy left at midrapidity to produce more charged hadrons.

Figure 12 shows that the prehydrodynamic flow has significant effects on the charged hadron anisotropic flow in p +Au collisions. At $p_T \approx 1$ GeV, the elliptic flow increases by 50% and triangular flow increases by 300% when we change from $\alpha^{\text{preflow}} = 0.15$ to $\alpha^{\text{preflow}} = 1.5$. The stronger sensitivity of

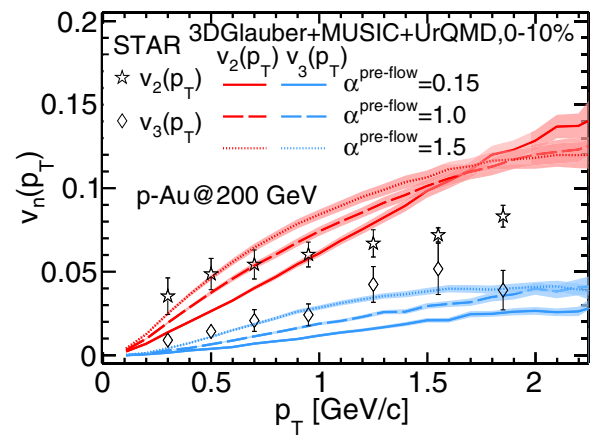


FIG. 12. The charged hadron anisotropic flow $v_n(p_T)$ as a function of p_T in central p +Au collisions with different values of α^{preflow} computed from the 3D-GLAUBER+MUSIC+URQMD framework. The results are compared to experimental data from the STAR Collaboration [21].

higher order anisotropic flow to prehydrodynamic flow is in qualitative agreement with early results from boost-invariant simulations [30]. With $\alpha^{\text{preflow}} = 1.5$, our simulations can

reproduce the STAR $v_3(p_T)$ data but they overestimate the $v_2(p_T)$ for $p_T > 0.6$ GeV at the same time. This result is in qualitative agreement with results shown in Ref. [74].

-
- [1] U. Heinz and R. Snellings, Collective flow and viscosity in relativistic heavy-ion collisions, *Annu. Rev. Nucl. Part. Sci.* **63**, 123 (2013).
- [2] C. Gale, S. Jeon, and B. Schenke, Hydrodynamic modeling of heavy-ion collisions, *Int. J. Mod. Phys. A* **28**, 1340011 (2013).
- [3] C. Shen and U. Heinz, The road to precision: Extraction of the specific shear viscosity of the quark-gluon plasma, *Nucl. Phys. News* **25**, 6 (2015).
- [4] C. Shen and L. Yan, Recent development of hydrodynamic modeling in heavy-ion collisions, *Nucl. Sci. Technol.* **31**, 122 (2020).
- [5] G. Aad *et al.* (ATLAS Collaboration), Two-particle azimuthal correlations in photonuclear ultraperipheral Pb+Pb collisions at 5.02 TeV with ATLAS, *Phys. Rev. C* **104**, 014903 (2021).
- [6] W. Zhao, C. Shen, and B. Schenke, Collectivity in ultraperipheral Pb+Pb collisions at the Large Hadron Collider, *Phys. Rev. Lett.* **129**, 252302 (2022).
- [7] C. Shen, W. Zhao, and B. Schenke, Collectivity in ultraperipheral heavy-ion collisions, in 20th International Conference on Strangeness in Quark Matter 2022 (unpublished), [arXiv:2209.15065](https://arxiv.org/abs/2209.15065).
- [8] K. Dusling, W. Li, and B. Schenke, Novel collective phenomena in high-energy proton-proton and proton-nucleus collisions, *Int. J. Mod. Phys. E* **25**, 1630002 (2016).
- [9] C. Loizides, Experimental overview on small collision systems at the LHC, *Nucl. Phys. A* **956**, 200 (2016).
- [10] S. Schlichting and P. Tribedy, Collectivity in small collision systems: An initial-state perspective, *Adv. High Energy Phys.* **2016**, 8460349 (2016).
- [11] J. L. Nagle and W. A. Zajc, Small system collectivity in Relativistic Hadronic and nuclear collisions, *Annu. Rev. Nucl. Part. Sci.* **68**, 211 (2018).
- [12] B. Schenke, C. Shen, and P. Tribedy, Hybrid color glass condensate and hydrodynamic description of the Relativistic Heavy Ion Collider small system scan, *Phys. Lett. B* **803**, 135322 (2020).
- [13] B. Schenke, The smallest fluid on Earth, *Rep. Prog. Phys.* **84**, 082301 (2021).
- [14] C. Aidala *et al.* (PHENIX Collaboration), Measurements of Multiparticle Correlations in $d + Au$ Collisions at 200, 62.4, 39, and 19.6 GeV and $p + Au$ Collisions at 200 GeV and Implications for Collective Behavior, *Phys. Rev. Lett.* **120**, 062302 (2018).
- [15] C. Aidala *et al.* (PHENIX Collaboration), Creation of quark-gluon plasma droplets with three distinct geometries, *Nat. Phys.* **15**, 214 (2019).
- [16] W. Li, Observation of a ‘Ridge’ correlation structure in high multiplicity proton-proton collisions: A brief review, *Mod. Phys. Lett. A* **27**, 1230018 (2012).
- [17] M. Habich, J. L. Nagle, and P. Romatschke, Particle spectra and HBT radii for simulated central nuclear collisions of C + C, Al + Al, Cu + Cu, Au + Au, and Pb + Pb from $\sqrt{s} = 62.4 - 2760$ GeV, *Eur. Phys. J. C* **75**, 15 (2015).
- [18] C. Shen, J.-F. Paquet, G. S. Denicol, S. Jeon, and C. Gale, Collectivity and electromagnetic radiation in small systems, *Phys. Rev. C* **95**, 014906 (2017).
- [19] M. Mace, V. V. Skokov, P. Tribedy, and R. Venugopalan, Hierarchy of Azimuthal Anisotropy Harmonics in Collisions of Small Systems from the Color Glass Condensate, *Phys. Rev. Lett.* **121**, 052301 (2018); **123**, 039901(E) (2019).
- [20] M. Mace, V. V. Skokov, P. Tribedy, and R. Venugopalan, Systematics of azimuthal anisotropy harmonics in proton-nucleus collisions at the LHC from the color glass condensate, *Phys. Lett. B* **788**, 161 (2019); **799**, 135006(E) (2019).
- [21] R. A. Lacey (STAR Collaboration), Long-range collectivity in small collision-systems with two- and four-particle correlations @ STAR, *Nucl. Phys. A* **1005**, 122041 (2021).
- [22] Measurements of the elliptic and triangular azimuthal anisotropies in central $^3\text{He} + \text{Au}$, $d + \text{Au}$ and $p + \text{Au}$ collisions at $\sqrt{s_{NN}} = 200$ GeV, [arXiv:2210.11352](https://arxiv.org/abs/2210.11352).
- [23] A. Adare *et al.* (PHENIX Collaboration), Pseudorapidity Dependence of Particle Production and Elliptic Flow in Asymmetric Nuclear Collisions of $p + \text{Al}$, $p + \text{Au}$, $d + \text{Au}$, and $^3\text{He} + \text{Au}$ at $\sqrt{s_{NN}} = 200$ GeV, *Phys. Rev. Lett.* **121**, 222301 (2018).
- [24] V. Khachatryan *et al.* (CMS Collaboration), Evidence for transverse momentum and pseudorapidity dependent event plane fluctuations in PbPb and $p\text{Pb}$ collisions, *Phys. Rev. C* **92**, 034911 (2015).
- [25] P. Bozek, A. Bzdak, and G.-L. Ma, Rapidity dependence of elliptic and triangular flow in proton-nucleus collisions from collective dynamics, *Phys. Lett. B* **748**, 301 (2015).
- [26] B. Schenke and S. Schlichting, 3D glasma initial state for relativistic heavy ion collisions, *Phys. Rev. C* **94**, 044907 (2016).
- [27] C. Shen and S. Alzhrani, Collision-geometry-based 3D initial condition for relativistic heavy-ion collisions, *Phys. Rev. C* **102**, 014909 (2020).
- [28] Z.-F. Jiang, S. Cao, X.-Y. Wu, C. B. Yang, and B.-W. Zhang, Longitudinal distribution of initial energy density and directed flow of charged particles in relativistic heavy-ion collisions, *Phys. Rev. C* **105**, 034901 (2022).
- [29] X.-Y. Wu and G.-Y. Qin, Asymmetric longitudinal flow decorrelations in proton-nucleus collisions, [arXiv:2109.03512](https://arxiv.org/abs/2109.03512).
- [30] P. Romatschke, Light-heavy ion collisions: A window into pre-equilibrium QCD dynamics? *Eur. Phys. J. C* **75**, 305 (2015).
- [31] C. Shen and B. Schenke, Longitudinal dynamics and particle production in relativistic nuclear collisions, *Phys. Rev. C* **105**, 064905 (2022).
- [32] IEBE-MUSIC is a general-purpose numerical framework to simulate dynamical evolution of relativistic heavy-ion collisions event-by-event. This work uses v0.5 of this framework, which can be downloaded from <https://github.com/chunshen1987/IEBE-MUSIC>.
- [33] C. Shen and B. Schenke, Dynamical initial state model for relativistic heavy-ion collisions, *Phys. Rev. C* **97**, 024907 (2018).
- [34] B. Schenke, S. Jeon, and C. Gale, Elliptic and Triangular Flow in Event-by-Event (3+1)D Viscous Hydrodynamics, *Phys. Rev. Lett.* **106**, 042301 (2011).
- [35] B. Schenke, S. Jeon, and C. Gale, (3+1)D hydrodynamic simulation of relativistic heavy-ion collisions, *Phys. Rev. C* **82**, 014903 (2010).

- [36] J.-F. Paquet, C. Shen, G. S. Denicol, M. Luzum, B. Schenke, S. Jeon, and C. Gale, Production of photons in relativistic heavy-ion collisions, *Phys. Rev. C* **93**, 044906 (2016).
- [37] G. S. Denicol, C. Gale, S. Jeon, A. Monnai, B. Schenke, and C. Shen, Net baryon diffusion in fluid dynamic simulations of relativistic heavy-ion collisions, *Phys. Rev. C* **98**, 034916 (2018).
- [38] MUSIC is the numerical implementation of (3+1)D relativistic viscous hydrodynamic simulations for high energy heavy-ion collisions. Its official website is <http://www.physics.mcgill.ca/music>. This work uses v2.5 of this framework, which can be downloaded from <https://github.com/MUSIC-fluid/MUSIC>.
- [39] S. A. Bass *et al.*, Microscopic models for ultrarelativistic heavy ion collisions, *Prog. Part. Nucl. Phys.* **41**, 255 (1998).
- [40] M. Bleicher *et al.*, Relativistic hadron hadron collisions in the ultrarelativistic quantum molecular dynamics model, *J. Phys. G: Nucl. Part. Phys.* **25**, 1859 (1999).
- [41] We use the official URQMD v3.4 and set it up to run as the afterburner mode, https://bitbucket.org/Chunshen1987/urqmd_afterburner/src/master/.
- [42] A. Bialas, A. Bzdak, and V. Koch, Stopped nucleons in configuration space, *Acta Phys. Pol. B* **49**, 103 (2018).
- [43] C. Shen and B. Schenke, Dynamical initialization and hydrodynamic modeling of relativistic heavy-ion collisions, *Nucl. Phys. A* **982**, 411 (2019).
- [44] A. Adare *et al.* (PHENIX Collaboration), Centrality categorization for $R_{p(d)+A}$ in high-energy collisions, *Phys. Rev. C* **90**, 034902 (2014).
- [45] J. Carlson and R. Schiavilla, Structure and dynamics of few nucleon systems, *Rev. Mod. Phys.* **70**, 743 (1998).
- [46] E. Schnedermann, J. Sollfrank, and U. W. Heinz, Thermal phenomenology of hadrons from 200A GeV S+S collisions, *Phys. Rev. C* **48**, 2462 (1993).
- [47] D. Teaney, J. Lauret, and E. V. Shuryak, Flow at the SPS and RHIC as a Quark-Gluon Plasma Signature, *Phys. Rev. Lett.* **86**, 4783 (2001).
- [48] U. W. Heinz, Concepts of heavy ion physics, in 2nd CERN-CLAF School of High Energy Physics, 2004 (unpublished), pp. 165–238, [arXiv:hep-ph/0407360](https://arxiv.org/abs/hep-ph/0407360).
- [49] M. Okai, K. Kawaguchi, Y. Tachibana, and T. Hirano, New approach to initializing hydrodynamic fields and mini-jet propagation in quark-gluon fluids, *Phys. Rev. C* **95**, 054914 (2017).
- [50] C. Shen, G. Denicol, C. Gale, S. Jeon, A. Monnai, and B. Schenke, A hybrid approach to relativistic heavy-ion collisions at the RHIC BES energies, *Nucl. Phys. A* **967**, 796 (2017).
- [51] L. Du, U. Heinz, and G. Vujanovic, Hybrid model with dynamical sources for heavy-ion collisions at BES energies, *Nucl. Phys. A* **982**, 407 (2019).
- [52] S. Borsanyi, Z. Fodor, S. D. Katz, S. Krieg, C. Ratti, and K. Szabo, Fluctuations of conserved charges at finite temperature from lattice QCD, *J. High Energy Phys.* **01** (2012) 138.
- [53] S. Borsanyi, Z. Fodor, C. Hoelbling, S. D. Katz, S. Krieg, and K. K. Szabo, Full result for the QCD equation of state with 2+1 flavors, *Phys. Lett. B* **730**, 99 (2014).
- [54] H. T. Ding, S. Mukherjee, H. Ohno, P. Petreczky, and H. P. Schadler, Diagonal and off-diagonal quark number susceptibilities at high temperatures, *Phys. Rev. D* **92**, 074043 (2015).
- [55] A. Bazavov *et al.*, The QCD equation of state to $\mathcal{O}(\mu_B^6)$ from lattice QCD, *Phys. Rev. D* **95**, 054504 (2017).
- [56] A. Monnai, B. Schenke, and C. Shen, Equation of state at finite densities for QCD matter in nuclear collisions, *Phys. Rev. C* **100**, 024907 (2019).
- [57] G. S. Denicol, H. Niemi, E. Molnar, and D. H. Rischke, Derivation of transient relativistic fluid dynamics from the Boltzmann equation, *Phys. Rev. D* **85**, 114047 (2012); **91**, 039902(E) (2015).
- [58] S. Ryu, C. Shen, B. Schenke (unpublished).
- [59] H. Mäntysaari, B. Schenke, C. Shen, and W. Zhao, Bayesian inference of the fluctuating proton shape, *Phys. Lett. B* **833**, 137348 (2022).
- [60] P. Huovinen and H. Petersen, Particlization in hybrid models, *Eur. Phys. J. A* **48**, 171 (2012).
- [61] C. Shen, Z. Qiu, H. Song, J. Bernhard, S. Bass, and U. Heinz, The iEBE-VISHNU code package for relativistic heavy-ion collisions, *Comput. Phys. Commun.* **199**, 61 (2016).
- [62] The iSS code package is an open-source particle sampler based on the Cooper-Frye freeze-out prescription. It converts fluid cells to particle samples. This work uses v1.0 of iSS, which can be downloaded from <https://github.com/chunshen1987/iSS/releases>.
- [63] S. Ryu, J. F. Paquet, C. Shen, G. S. Denicol, B. Schenke, S. Jeon, and C. Gale, Importance of the Bulk Viscosity of QCD in Ultrarelativistic Heavy-Ion Collisions, *Phys. Rev. Lett.* **115**, 132301 (2015).
- [64] S. Ryu, J.-F. Paquet, C. Shen, G. Denicol, B. Schenke, S. Jeon, and C. Gale, Effects of bulk viscosity and hadronic rescattering in heavy ion collisions at energies available at the BNL Relativistic Heavy Ion Collider and at the CERN Large Hadron Collider, *Phys. Rev. C* **97**, 034910 (2018).
- [65] B. I. Abelev *et al.* (STAR Collaboration), Systematic measurements of identified particle spectra in pp , d^+ Au and Au+Au Collisions from STAR, *Phys. Rev. C* **79**, 034909 (2009).
- [66] A. Bilandzic, R. Snellings, and S. Voloshin, Flow analysis with cumulants: Direct calculations, *Phys. Rev. C* **83**, 044913 (2011).
- [67] A. Bilandzic, C. H. Christensen, K. Gulbrandsen, A. Hansen, and Y. Zhou, Generic framework for anisotropic flow analyses with multiparticle azimuthal correlations, *Phys. Rev. C* **89**, 064904 (2014).
- [68] C. Aidala *et al.* (PHENIX Collaboration), Measurements of azimuthal anisotropy and charged-particle multiplicity in d +Au collisions at $\sqrt{s_{NN}} = 200, 62.4, 39,$ and 19.6 GeV, *Phys. Rev. C* **96**, 064905 (2017).
- [69] U. A. Acharya *et al.* (PHENIX Collaboration), Kinematic dependence of azimuthal anisotropies in p +Au, d +Au, and ^3He +Au at $\sqrt{s_{NN}} = 200$ GeV, *Phys. Rev. C* **105**, 024901 (2022).
- [70] U. A. Acharya *et al.* (PHENIX Collaboration), Measurements of second-harmonic Fourier coefficients from azimuthal anisotropies in p + p , p +Au, d +Au, and ^3He +Au collisions at $\sqrt{s_{NN}} = 200$ GeV, [arXiv:2203.09894](https://arxiv.org/abs/2203.09894).
- [71] A. Adare *et al.* (PHENIX Collaboration), Multiparticle azimuthal correlations for extracting event-by-event elliptic and triangular flow in Au+Au collisions at $\sqrt{s_{NN}} = 200$ GeV, *Phys. Rev. C* **99**, 024903 (2019).
- [72] R. Pordes *et al.*, The Open Science Grid, *J. Phys.: Conf. Ser.* **78**, 012057 (2007).
- [73] I. Sfiligoi, D. C. Bradley, B. Holzman, P. Mhashilkar, S. Padhi, and F. Wurthwein, The pilot way to grid resources using glidein-WMS, *WRI World Congr.* **2**, 428 (2009).
- [74] B. Schenke, C. Shen, and P. Tribedy, Running the gamut of high energy nuclear collisions, *Phys. Rev. C* **102**, 044905 (2020).